Supporting Information

Interferometric Plasmonic Imaging and Detection of Single Exosomes

Yuting Yang[1], Guangxia Shen[1], Hui Wang[2], Hongxia Li[1], Ting Zhang[1], Nongjian Tao[2,3], Xianting Ding[1,4*], Hui Yu[1*]

1. Institute for Personalized Medicine, School of Biomedical Engineering, Shanghai Jiao Tong University, Shanghai 200030, China

2. State Key Laboratory of Analytical Chemistry for Life Science, School of Chemistry and Chemical Engineering, Nanjing University, Nanjing 210093, China

3. Biodesign Center for Bioelectronics and Biosensors, Arizona State University, Tempe, AZ 85287, USA

4. State Key Laboratory of Oncogenes and Related Genes, Shanghai Jiao Tong University, Shanghai, 200030, China

* Correspondence should be sent to:

Prof. Hui Yu,

1954 Huashan Road, MED-X Institute Building, #416, Shanghai, 200030, China

hui.yu@sjtu.edu.cn; +86-21-62933948

or Prof. Xianting Ding

dingxianting@sjtu.edu.cn; +86-15601752012

www.pnas.org/cgi/doi/10.1073/pnas.1804548115

1. Image-processing and reconstruction algorithms

The workflow of image-processing algorithms is shown in Fig. S1 (1). The first image (background image) was subtracted from the whole image sequence, and then processed with a running-average algorithm (N=32). 30 images with visible 100-nm nanoparticles were selected from an image sequence and averaged, and the resulting image was 2-D Fourier transformed into *k*-space. The wave vector of the SPs was then determined by fitting one of the rings in *k*-space and calculating the center and radius with a Matlab code. We simulated the reflected light in Eq. 1 as a planar wave, because the incident light was collimated and refocused as a parallel light.

The realization of the image-reconstruction algorithm is through obtaining the scattered field E_{sc} after multiplying the image with the simulated reflected light field, as in Eq. S1.

$$\mathrm{dI}\cdot E_{\mathrm{ref}} = |E_{\mathrm{sc}}|^2 E_{\mathrm{ref}} + |E_{\mathrm{ref}}|^2 E_{\mathrm{sc}} + {E_{\mathrm{ref}}}^2 {E_{\mathrm{sc}}}^* \tag{S1}$$

where $|E_{\mathrm{sc}}|^2 E_{\mathrm{ref}}$ is negligible, and $|E_{\mathrm{ref}}|^2 E_{\mathrm{sc}}$ and ${E_{\mathrm{ref}}}^2 {E_{\mathrm{sc}}}^*$ corresponds to the two rings in *k*-space. The two rings could thus be separated with a spatial mask filter, leaving only the $|E_{\mathrm{ref}}|^2 E_{\mathrm{sc}}$ component. The scattered field E_{sc} is further deconvolved by the scattered field of a 100-nm silica nanoparticle experimentally determined.

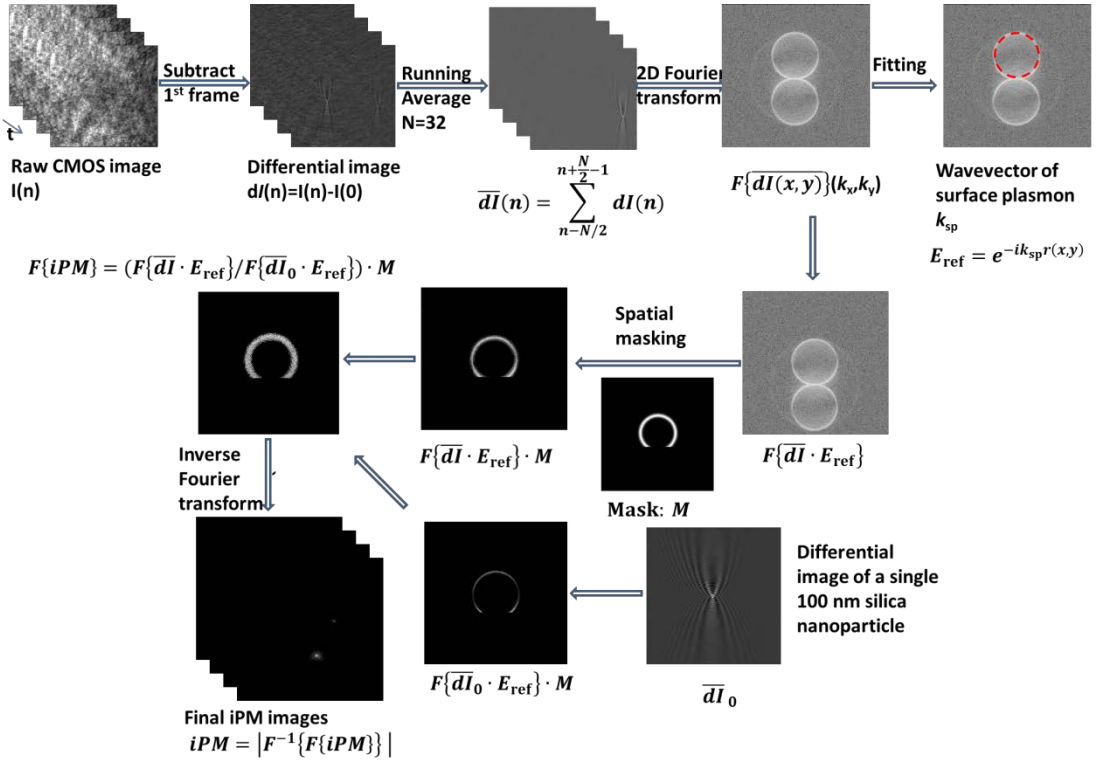

Fig. S1 Workflow of the iPM image-processing and reconstruction algorithms

2. Signal-to-noise ratio (SNR) improvement with running-average algorithms

As in Fig. S2a, the SNR was defined as the difference between peak intensity and mean background intensity, divided by the standard deviation of the background noise. The iPM image intensity of a silica or exosome nanoparticle was calculated as the mean intensity of a 3×3-pixel area around the peak pixel (insets), after subtracting the mean background intensity. Fig. S2b

shows the line profile of a 100-nm silica nanoparticle, with different number of images (*N*) used in the running-average algorithms.

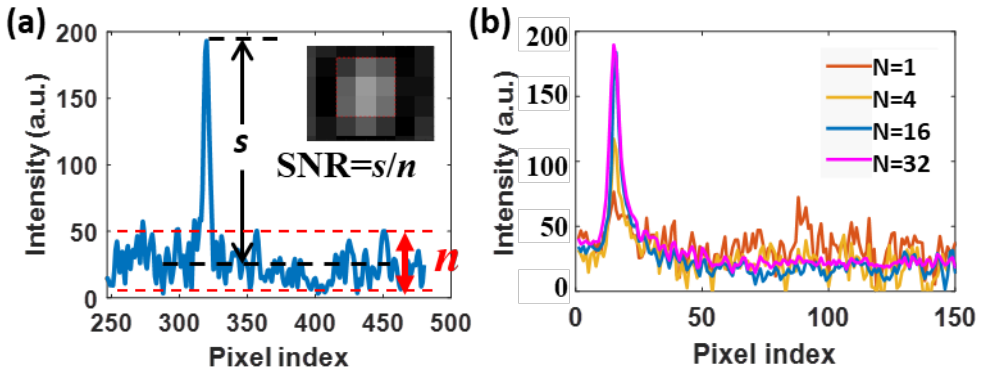

Fig. S2 Improving SNR with the running-average algorithm. (a) Definition of the SNR and image intensity in iPM; (b) line profiles across the iPM image of a 100-nm silica nanoparticle with different number of images (*N*) used in the running-average algorithm.

3. The incident angle of iPM

The reflective light intensity is highly dependent on the incident angle, known as the surface plasmon resonance (SPR) phenomenon, as simulated in Fig. S3 with Matlab. The incident light for iPM experiments was set to the incident angle where 10% of the incident light was reflected, as indicated by the arrow.

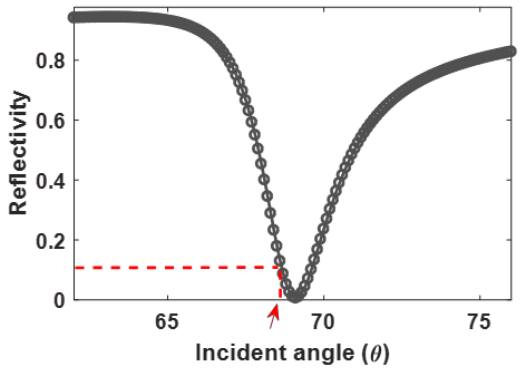

Fig. S3 Simulated reflectivity at different incident angle. Incident angle for iPM experiments was set at 10% reflection point as indicated by the arrow.

4. Numerical model of iPM intensity vs. particle size

The iPM intensity of a nanoparticle is expected to be proportional to the volume of the particle exposed in the evanescent field associated with the propagating surface plamson. Considering that the evanescent field *E* decays exponentially with distance from the surface, we express the intensity as

$$\mathrm{I} = C + k\int_0^{2r} \pi(2rz - z^2)\, e^{-z/l} dz \qquad \text{(S1)}$$

where *C* and *k* are constants (fitting parameter), *z* is distance above the gold surface, *r* is radius of the particle, and l is the decay constant of the evanescent field, which is approximately 200 nm.

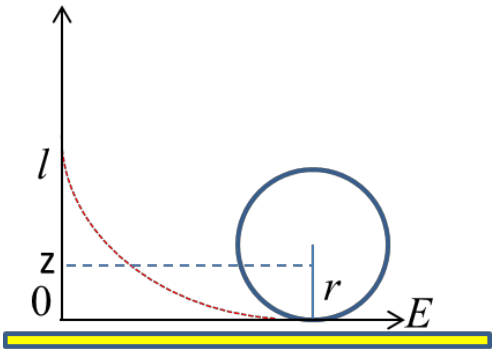

Fig. S4 Theoretical model of iPM intensity vs. particle size.

5. Typical TEM image of exosome and cationic liposome samples

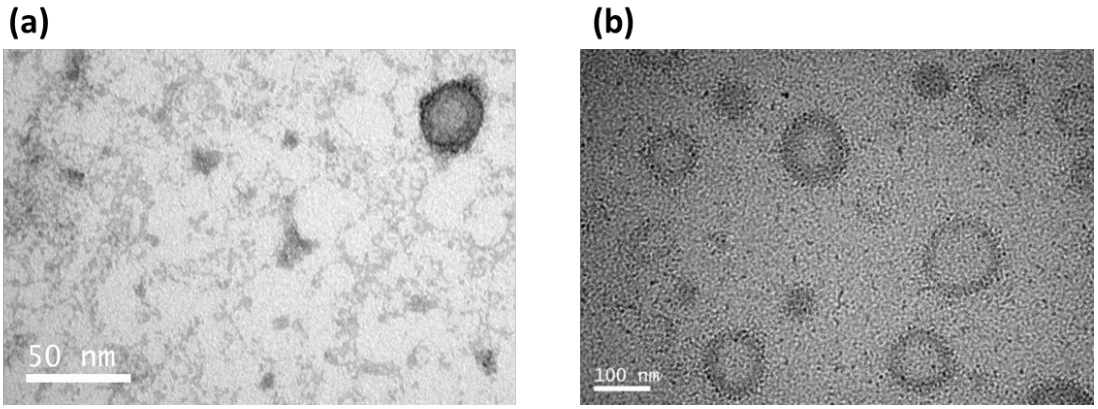

Fig. S5 TEM image of exosomes (a) and cationic liposomes (b). Note the characteristic teapot shape of an exosome.

6. Zeta potential of exosome and liposome samples

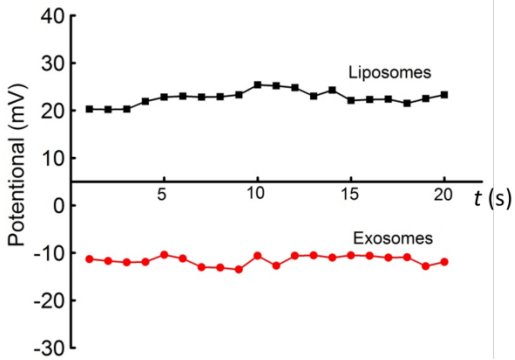

Fig. S6 Zeta potential of exosome and liposome samples. x axis represents time (s).

7. Analyzing size distribution of exosomes, cationic liposomes, and exosome/liposome complex after membrane fusion with NTA

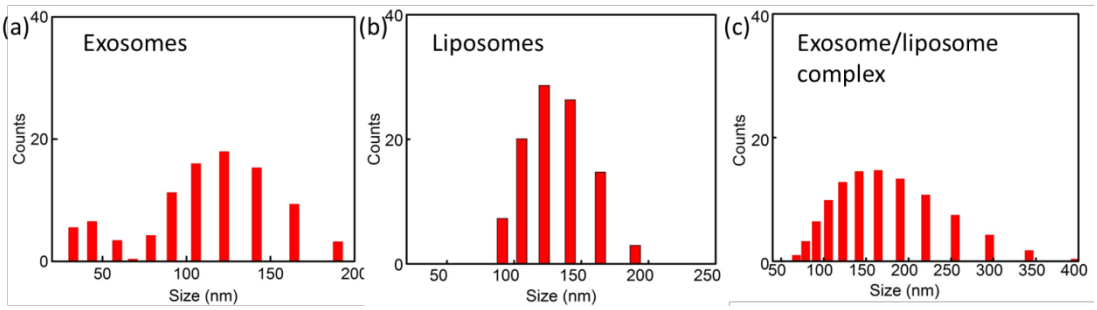

Fig. S7 Size distribution of exosomes (a), cationic liposomes (b), and exosome/liposome complex after membrane fusion at ratio E/L=2:1 determined by NTA analysis. Mean size of particles detected increased from ~125 nm (exosomes, liposomes) to ~170 nm after membrane fusion.

8. iPM study of exosome-liposome complex

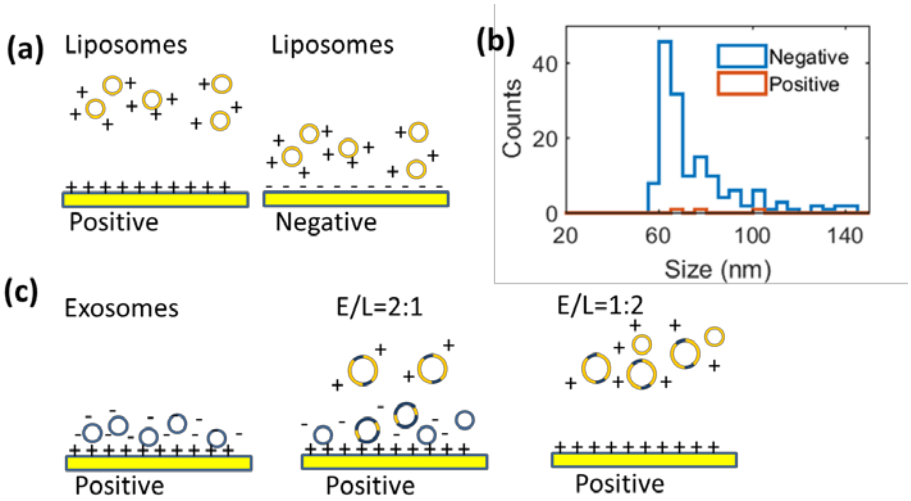

Fig. S8 Quantitative study of exosome-liposome membrane fusion with iPM. (a) Schematic of liposome adsorption on positive- or negative-charge-modified Au surface; (b) size distribution of liposomes adsorbed onto positive- or negative-charge-modified Au surface; (c) schematic of exosome-liposome complex absorption onto a positive-charge-modified Au surface. The net surface charge of the exosome-liposome complex was dependent on the concentration ratios between exosomes and liposomes during the membrane fusion process.

Movie.S1 Real-time adsorption of exosomes onto a positive-charge-modified Au surface.

Movie.S2 'hit-stay-run' behavior of an exosome bond to a CD 63 antibody-coated Au surface.

Reference

1. Yu H, Shan X, Wang S, & Tao N (2017) Achieving high spatial resolution surface plasmon resonance microscopy with image reconstruction. *Analytical Chemistry* 89(5):2704-2707.